Journal of Neuroradiology 46 (2019) 281–287

Available online at ScienceDirect www.sciencedirect.com

Elsevier Masson France EM|consulte www.em-consulte.com

Original Article

Presurgical differentiation between malignant haemangiopericytoma and angiomatous meningioma by a radiomics approach based on texture analysis

Xuanxuan Li [a], Yiping Lu [a], Ji Xiong [b], Dongdong Wang [a], Dejun She [a], Xinping Kuai [a], Daoying Geng [a,*], Bo Yin [a,*]

[a] Department of Radiology, Huashan Hospital Affiliated to Fudan University, 12 Wulumuqi Rd. Middle, Shanghai 200040, China
[b] Department of Pathology, Huashan Hospital Affiliated to Fudan University, 12 Wulumuqi Rd. Middle, Shanghai 200040, China

ARTICLE INFO

Article history:
Available online 18 June 2019

Keywords:
Magnetic resonance imaging
Meningioma
Haemangiopericytoma
Machine-learning
Support vector machine

ABSTRACT

Purpose. – To assess whether a machine-learning model based on texture analysis (TA) could yield a more accurate diagnosis in differentiating malignant haemangiopericytoma (HPC) from angiomatous meningioma (AM).
Materials and methods. – Sixty-seven pathologically confirmed cases, including 24 malignant HPCs and 43 AMs between May 2013 and September 2017 were retrospectively reviewed. In each case, 498 radiomic features, including 12 clinical features and 486 texture features from MRI sequences (T2-FLAIR, DWI and enhanced T1WI), were extracted. Three neuroradiologists independently made diagnoses by vision. Four Support Vector Machine (SVM) classifiers were built, one based on clinical features and three based on texture features from three MRI sequences after feature selection. The diagnostic abilities of these classifiers and three neuroradiologists were evaluated by receiver operating characteristic (ROC) analysis.
Results. – Malignant HPCs were found to have larger sizes, slighter degrees of peritumoural oedema compared with AMs ($P < 0.05$), and more serpentine-like vessels. The AUC of the enhanced T1WI-based classifier was 0.90, significantly higher than that of T2-FLAIR-based or DWI-based classifiers (0.77 and 0.73). The AUC of the SVM classifier based on clinical features was 0.66, slightly but not significantly lower than the performances of 3 neuroradiologists (AUC = 0.69, 0.70 and 0.73).
Conclusion. – Machine-learning models based on clinical features alone could not provide a better diagnostic performance than that of radiologists. The SVM classifier built by texture features extracted from enhanced T1WI is a promising tool to differentiate malignant HPC from AM before surgery.

Abbreviations

HPC	haemangiopericytoma
SFT/HPC	solitary fibrous tumour/haemangiopericytoma
CNS	central nervous system
AM	angiomatous meningioma
WHO	World Health Organization
TA	texture analysis
ADC	apparent diffusion coefficient
FLAIR	fluid attenuated inversion recovery
DWI	diffusion-weighted imaging
EPI-DWI	echo-planar diffusion-weighted imaging
SVM	support vector machine
ROI	region of interest
SD	standard deviation
ROC curve	receiver operating characteristic curve
AUC	area under curve
DICOM	digital imaging and communications in medicine
VEGF	vascular endothelial growth factor

Introduction

Haemangiopericytoma (HPC) is a rare tumour with a vascular origin [1]. Solitary fibrous tumour/haemangiopericytoma (SFT/HPC) became one entity in 2016 WHO classification [2]. WHO grade II and III tumours are characterized by the HPC phenotype with a malignant nature [3]. Only these are discussed in this

* Corresponding authors.
E-mail addresses: GengdaoyingGDY@163.com (D. Geng), yinbo9@163.com (B. Yin).

https://doi.org/10.1016/j.neurad.2019.05.013
0150-9861/

study. Malignant HPCs are known for aggressiveness, high rates of recurrence and systematic metastases. In radiological images, HPC mimics angiomatous meningioma (AM) that is usually benign [4]. Therefore, their treatment principles are largely different thus the presurgical differential diagnosis is crucial.

Differences in clinical and radiological characteristics have been reported to help identify them. HPCs usually have a male predominance and an earlier age of onset [5]. Radiologically, HPCs exhibit more aggressive behaviours like bone erosions or necrosis, low ADC values and heterogenous enhancement [6,7]. However, these features are not always effective, and the variability in interpretation is inevitable since it depends on vision.

Recently, radiomics has exhibited a promising ability in disease diagnosis by analysing large amounts of quantitative imaging features with a high throughput [8]. As a method of radiomics, texture analysis (TA) enables quantification and analysis of the grey-level patterns, pixel correlations, etc. [9]. Compared with a visual assessment, TA provides more objective and sensitive information, thus has potential in multiple clinical challenges especially medical image interpretation [10,11].

To our knowledge, no existing studies were found that explored the value of TA in distinguishing HPC and AM. Here, we quantified the difference between these two entities on the basis of T2-FLAIR, DWI and enhanced T1WI by means of TA to evaluate its diagnostic effectiveness. We investigated:

- whether TA would be more effective in differentiating HPC and AM than radiologists;
- the best MRI sequence for clinical practice.

Materials and methods

This was a retrospective study. Approval from the institutional review board (IRB) was obtained, and written informed consents were waived.

The schematic workflow is depicted in Fig. 1.

Patient cohort

In total, 119 consecutive patients with pathologically confirmed HPC and AM between May 2013 and September 2017 in our institution were reviewed. Preoperative enhanced MRI images were collected. Exclusion criteria included: previous relevant treatment history ($n = 12$); other severe neurological diseases ($n = 9$); incomplete MRI images or obvious motion artefacts ($n = 31$).

Finally, 43 patients with AM and 24 patients with HPC were included. Out of the 24 HPCs, 17 (70.8%) were graded as WHO grade II, and 7 (29.2%) as grade III. The mean (± SD) age of all the patients was 54.1 ± 13.0 years, and females accounted for 59.7% (Table 1).

A neuropathologist with 12 years' experience assessed all the pathological tumour slices according to the 2016 WHO classification system [2]. For confusing cases, a second opinion was provided by a senior neuropathologist for the final diagnosis.

MRI protocol

All patients experienced an MRI-enhanced head scan with the same 3.0T device (DISCOVERY MR750W, G.E, Milwaukee, MI, USA) with an 8-channel phased array head coil. The parameters of MRI sequences are listed in Supplementary Table. Enhanced T1WI were acquired 1 minute after injecting gadolinium-based contrast.

All images used in the study were available in a digital format. Semantic features (tumor characteristics assessed visually by radiologists) were also investigated. They were evaluated on a GE post-processing station (AW Volume Share^{TM} 5) by two radiologists blinded to the histopathological diagnosis after negotiation. Details of the all features were described in Table 2.

Three types of intratumoural vessels were observed. "Spot-shaped vessels" were small round voids of vessels. "Root-like vessels" were clusters of vessels that resemble tree roots. "Serpentine-like vessels" were the distorted and aberrant vessels.

ROIs for the ADC values were drawn by another radiologist. The solid-appearing portions of AM and HPC were selected. Both the ADC value and the area of the ROI in each slice were recorded, and the average ADC value for each patient was calculated.

Radiologist evaluation

Three neuroradiologists that were unaware of the pathological results independently reviewed the images. They made assessments on a 1-5 scale: 1 = definite AM, 2 = likely AM, 3 = not sure, 4 = likely HPC, 5 = definite HPC. Receiver operating characteristic (ROC) curves were drawn for the diagnosis of all three radiologists, and the area under curve (AUC) values were calculated.

Texture Feature Extraction

The MRI images were imported into a dedicated TA software MaZda (version 4.6) [12]. The N4 bias correction method was applied [13]. A polygonal ROI was drawn to segment the contrast-enhanced tumour region based on the enhanced T1WI, and copied to T2-FLAIR and DWI with the same axial level. Grey-level normalization and image quantization were performed (Supplementary Fig. 1). Grey-level normalization used the limitation of dynamics to $\mu \pm 3SD$ (μ, grey-level mean) [12]. Quantization of the resulting grey-level range was performed to compress the image between 1 and 2 k, where k is the number of bits per pixel [14]. The extracted features included grey-level histogram, co-occurrence matrix, run-length matrix, autoregressive model and wavelet transform. Altogether, 162 texture features were retrieved from 3 MRI sequence respectively (Table).

Texture feature selection

Feature selection was completed by R software (version 3.5.0). First, a temporal split was used randomly to assign the data to a training dataset and a testing set with a ratio of 0.7:0.3. Feature selection was based on the training dataset. All features were sequentially exported into R software to select the optimal features by an all-relevant selection with 'Boruta' package [15]. Finally, 11 texture features from T2-FLAIR, 24 from DWI and 21 from enhanced T1WI were confirmed to be important in differentiating AM and HPC and were selected for further calculation. Among them, "X45dgr_GlevNonU" was of the highest importance in T2-FLAIR (HPC: AM = 866.6: 468.8) and DWI (HPC: AM = 669.7: 374.8), so was "Vertl_GlevNonU" in T1WI (HPC: AM = 615.3: 287.1).

Classification

Classification was performed using R software. Since differentiation between AM and HPC was a binary problem, Support Vector Machine (SVM) classifiers were built. Nested cross validation was used for model tuning and training by "caret" package on the training set [16]. Differences in the predictive power among the models were assessed using bootstrapping (1000 iterations). A total of 4 SVM models were built, one based on "clinical features" and the other three based on texture features selected from T2-FLAIR, DWI and enhanced T1WI. The "clinical features" model is a machine-learning outcome from both semantic features and clinical characteristics including age, gender, etc. The diagnostic

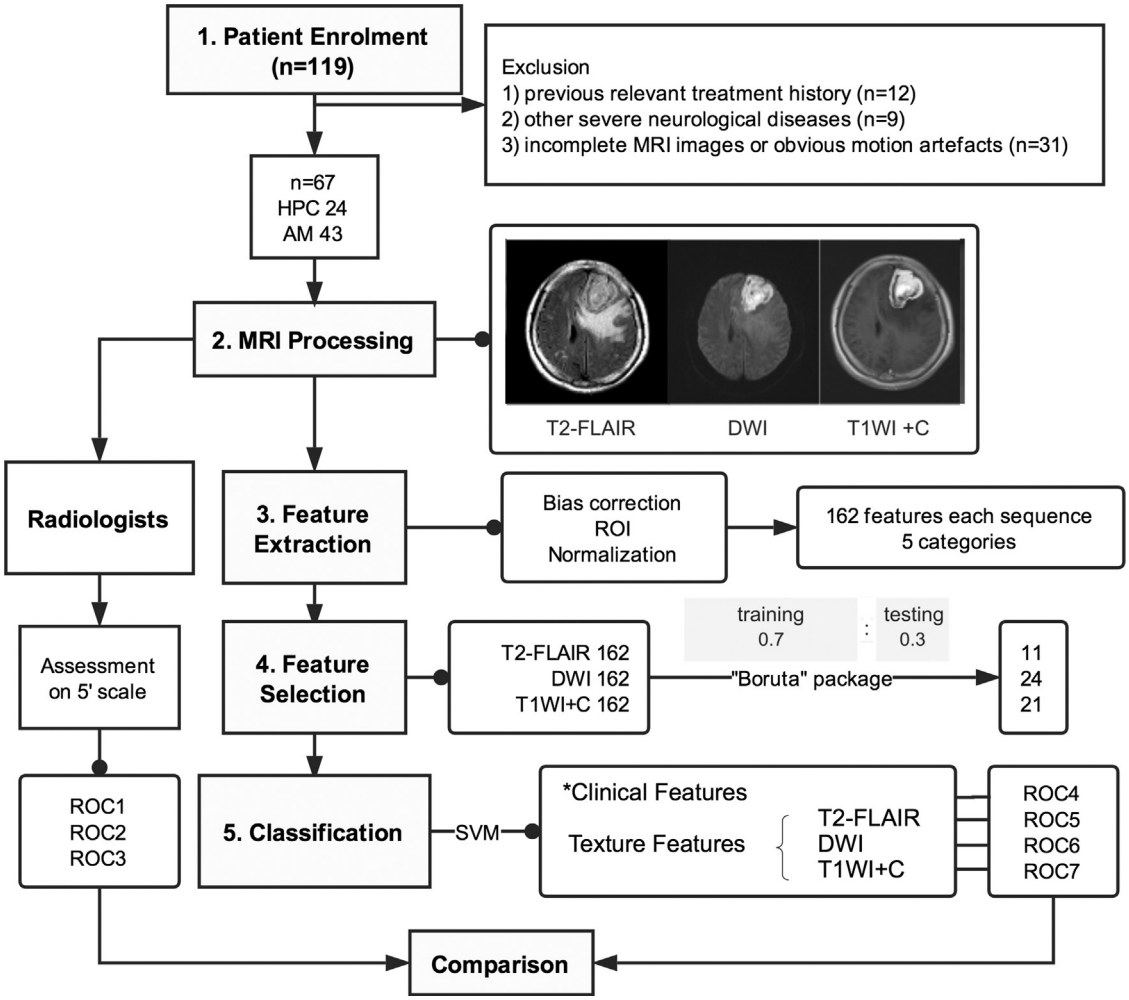

Fig. 1. Flowchart of the whole study. *Clinical features were obtained from clinical and semantic characteristics.

Table 1
Baseline information of patients enrolled.

	HPC	AM	*P*-value	Total
Number of patients	24	43	–	67
Number of slices in each sequence	117	149	–	266
Female (*n*,%)	13 (54.17%)	27 (62.79%)	0.5665	40 (59.70%)
Age (year)	47.34 ± 14.28	57.93 ± 11.03	0.0089	54.14 ± 12.97
Location (*n*, %)				
Cerebral convexity	10 (41.67%)	25 (58.13%)	0.0531[a]	35 (52.24%)
Falx	3 (12.50%)	11 (25.58%)		14 (20.90%)
Skull base	9 (37.50%)	6 (13.95%)		15 (22.39%)
Others	2 (8.33%)	1(2.33%)		3 (4.48%)
Recurrence (*n*, %)	3 (13.04%)	1 (2.33%)	0.1180[a]	4 (5.97%)
Death (*n*, %)	3 (13.04%)	0 (0%)	0.0390[a]	3 (4.48%)
Ki-67 value (%)	10.74 ± 7.50	1.88 ± 1.28	< 0.0001	4.97 ± 6.18

AM: angiomatous meningioma.
[a] Fisher exact test (Chi^2 test).

efficiency of each SVM classifier was subsequently testified by the data from the testing dataset with a ROC analysis.

Statistical analysis

All statistical analyses were performed using R software. The significance and correlations of the non-continuous features were evaluated using Chi^2 test and Fisher's exact test. The continuous data among clinical and texture features were presented as the mean ± standard deviation (SD) and compared using T test. AUC values from the ROC curves were compared using a DeLong test.

Results

Clinical information

HPC patients were found to be younger than AM (47.3 ± 14.3 versus 57.9 ± 11.0, $P = 0.009$). By the time of our follow-up in July 2018, three out of 24 HPC patients had at tumor recurrence, and

Table 2
The description of all features.

Feature/parameter	Description
Clinical information	
Age	Age difference between HPC and AM
Gender	Gender difference between HPC and AM
Location	Including convexity, falx and skull base
Semantic features	
Maximum diameter	The maximum length of the tumours
Irregularity	Irregularities in the shape or border of the tumours
Cystic component	Cyst composition filled with fluid in the tumours
Necrosis/haemorrhage	Presence of necrosis or haemorrhages in the tumours
Bony invasion	Appearance of tumour invading the adjacent skull
Hyperostosis	Excessive growth of bone adjacent to the tumours
Peritumoural oedema	Area and severity of the oedema around the tumours
Multifocal lesions	Growth of tumours in multiple sites
Dural tail sign	Thickening and enhancement of the dura
Existence of vessels	Existence of intratumoural vessels
ADC values	
Mean ADC values	The apparent diffusion coefficient based on signal intensity acquired on DWI maps with b = 0 and b = 1000 s/mm^2
Radiomic features	
Grey-level histogram	First-order statistical features computed from the intensity of pixels in the images with gray levels
Co-occurrence matrix	Second-order statistical features to explore the spatial relationship between 2 pixels with certain distance and direction, including contrast, correlation, entropy, angular second moment, etc.
Run-length matrix	A matrix to explore the number of pixels with same gray level as the first one in certain direction, including long-run emphasis, short-run emphasis, etc.
Autoregressive model	The model assumes that pixel intensity, in reference to the mean value of image intensity, may be predicted as a weighted sum of four neighboring pixel intensities
Wavelet transform	A kind of transformation that separates data into different frequency components, and then studies each component with resolution matched to its scale

AM: angiomatous meningioma; ADC: apparent diffusion coefficient.

Table 3
Difference between AM and HPC in semantic features.

	HPC(n = 24)	AM (n = 43)	P-value
Maximum diameter (cm)	5.30 ± 1.90	3.83 ± 1.27	0.0004
Irregular shape	12 (50.00%)	17 (39.53%)	0.3318
Cystic composition	5 (20.83%)	10 (23.26%)	0.8907
Necrosis or hemorrhage	13 (54.16%)	23 (53.49%)	0.8170
Bony invasion	9 (37.50%)	5 (11.63%)	0.0087
Hyperostosis	5 (20.83%)	25 (58.14%)	0.0042
Multifocal lesions	2 (8.33%)	1 (2.33%)	0.2430
Dural tail sign	10 (41.67%)	27 (62.79%)	0.1361
Existence of vessels	13 (54.16%)	20 (46.51%)	0.8170
Vessel morphology			
Root-like	2 (8.33%)	8 (18.60%)	0.0053
Spot-shaped	5 (20.83%)	12 (27.91%)	
Serpentine-like	6 (25.00%)	0	
Peritumoural edema			
None/mild	14 (58.33%)	12 (27.91%)	0.0222
Moderate/severe	10 (41.67%)	31 (72.09%)	

AM: angiomatous meningioma.

three died. The numbers in the AM group were one out of 43 and none. Other baseline information are shown in Table 1.

Difference between HPC and AM in semantic features

The semantic features were observed and analysed (Table 3). HPC lesions were larger than AM (5.3 ± 1.9 cm versus 3.8 ± 1.3 cm). Although the existence of vessels could not help with differentiation (P > 0.05), the shapes of the vessels were found to be different (P = 0.005) (Fig. 2). HPCs displayed more serpentine-like vessels, while AM showed mostly root-like vessels. 58.3% of the HPCs had none to mild oedema, while 72.1% of the AMs had moderate to severe oedema (P = 0.04). More HPC lesions eroded the adjacent bone (P = 0.009), and AM lesions were more associated with bony hyperostosis (P = 0.004). Other semantic features showed no significant differences (P > 0.05).

All the aforementioned parameters with ADC value, age and gender are shown in the matrix plot in Fig. 3 to disclose the correlations between each other.

Diagnostic performances of neuroradiologists

Three radiologists achieved a similar diagnostic performance with AUC values of 0.69, 0.70, and. The accuracies were 66.7%, 72.7%, and 77.3%, respectively.

Two representative confusing cases are presented in Supplementary Fig. 2.

Diagnostic performances of 4 SVM classifiers

The AUCs and 95% CI of the SVM classifiers based on T2-FLAIR, DWI, and enhanced T1WI, were 0.77 (0.66–0.87), 0.73 (0.62-0.84) and 0.90 (0.82–0.98), with accuracies of 77.50%, 68.75% and 87.50%, respectively. Additionally, the SVM classifier built by clinical features alone exhibited a low AUC value of 0.66 (0.37–0.95).

All the ROC curves are presented in Fig. 4. Only the SVM classifier based on enhanced T1WI showed a significantly better performance than others.

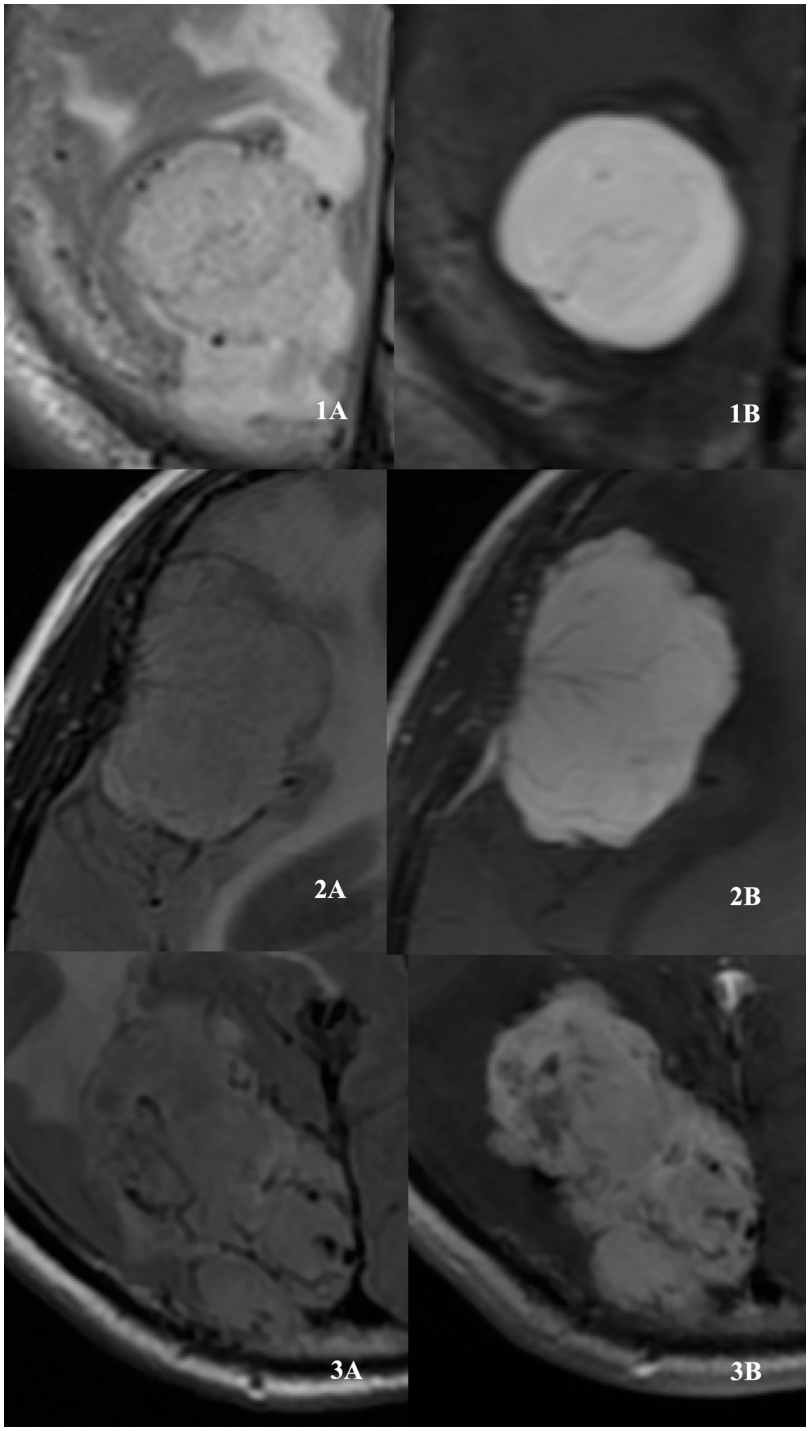

Fig. 2. Illustration of vessel morphology [19]. 1A–1B spot-shaped vessels: some small and round void of vessels are seen around the tumour in T2-FLAIR and enhanced T1W images. 2A–2B root-like vessels: a cluster of vessels are observed in the outer portion of lesion which resembles tree root. 3A–3B Serpentine-like vessels: the distorted and aberrant vessels inside the tumour are more usually seen in HPCs than angiomatous meningiomas (AMs).

Discussion

Malignant HPC are hardly distinguishable radiologically from AMs, which are mostly benign [17]. Preoperative differentiation between HPC and AM is crucial for suitable treatment plans.

We found some clues that might help to distinguish them. First, HPC had a lower age of onset and a larger tumour size. These indicated a rapid growth and a short duration in HPC [18]. Second, peritumoural oedema was slighter in HPCs. The intratumoural vasculature of AM with thicker walls and thinner lumens results in relatively stronger vascular resistance and slower blood flow, which causes obvious vasogenic oedema [6]. Third, HPC lesions displayed more serpentine-like vessels, and AM showed more root-like vessels which was aligned with previously reported “sunburst sign” [19]. It was reported that the major feeder vessels of HPCs came from the internal carotid artery or the posterior cerebral arteries, while the major supply to AM was from meningeal arteries stemming from the external carotid artery [20,21]. The latter arteries excessively grew through the tumor and splitted into branches.

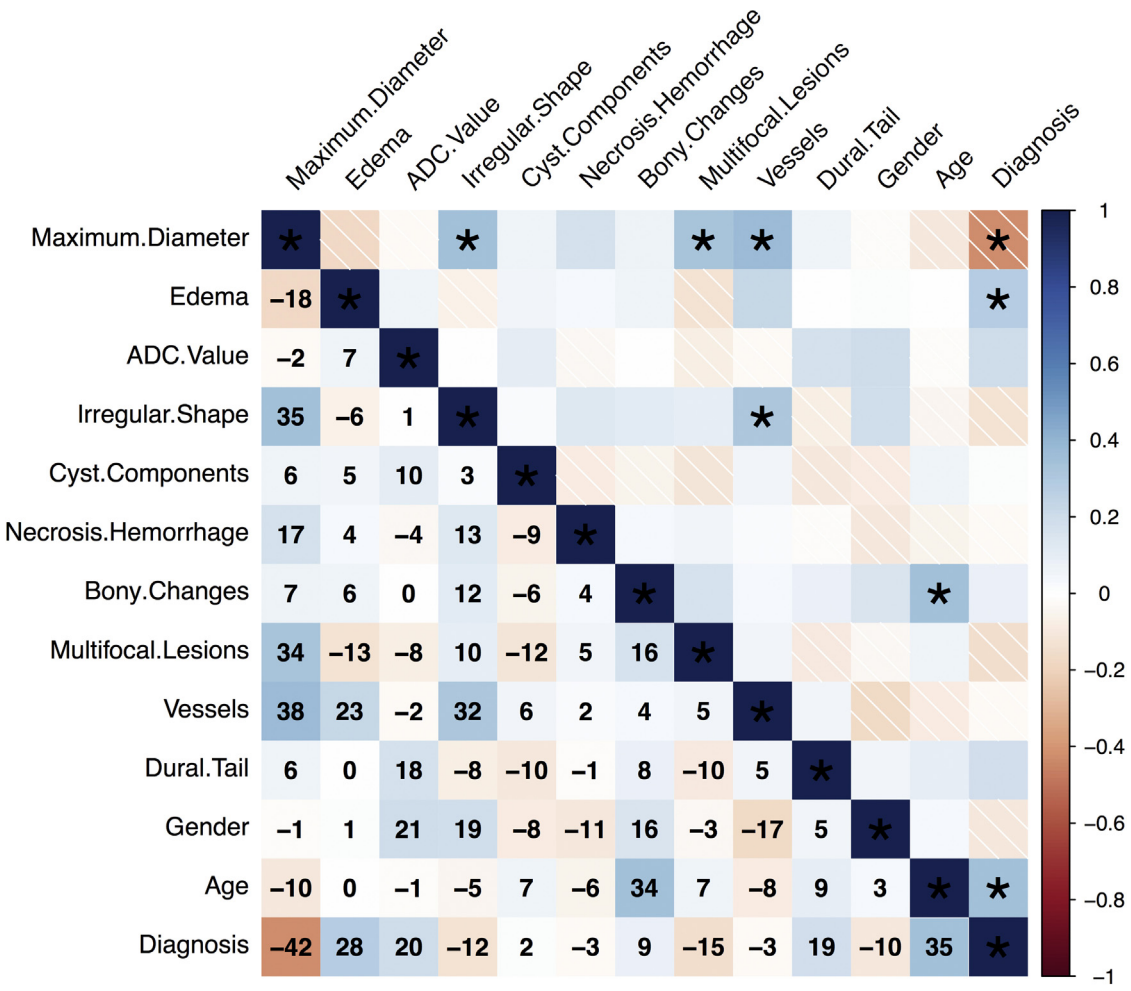

Fig. 3. Matrix plot of correlation among morphological and clinical parameters. The range of correlation coefficients (CCs) is between −1 to 1. The numbers in the figure are CCs*100 for the convenience of display. *$P < 0.05$.

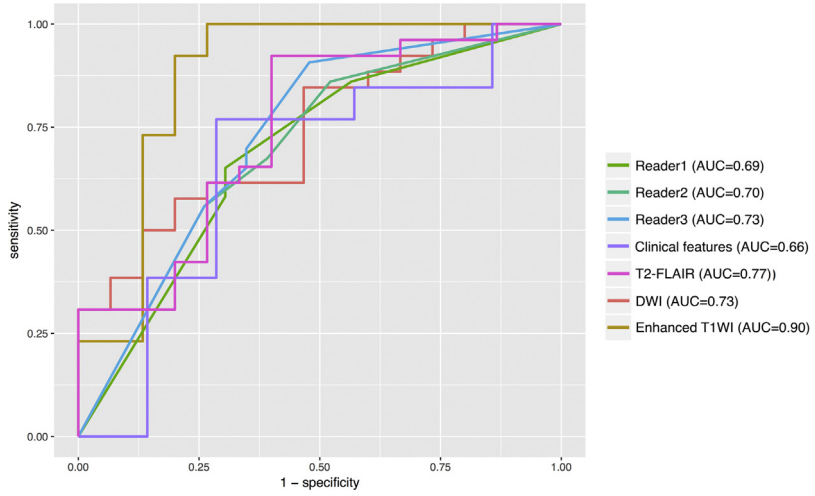

Fig. 4. Receiver operating characteristic (ROC) analysis of 3 radiologists and 4 Support Vector Machine (SVM) classifiers.

The differences in bony changes were compliant with previous studies. Unlike AMs that usually show hyperostosis, HPCs show more bone invasion [22].

We extracted texture information from conventional MRI and performed TA, expecting to detect differences that were not observable by vision. The SVM classifier based on enhanced T1WI yielded excellent performance. Its AUC reached as high as 0.90 (95% CI: 0.82–0.98) with satisfying sensitivity, specificity and accuracy, indicating a better diagnostic value than other sequences or radiologists. These results indicated that TA, as opposed to visual analyses, is capable of improving the differential diagnosis between HPC and AM, especially with enhanced T1WI. TA could be widely

applied since these conventional sequences are routinely performed.

In addition, the SVM classifier of the clinical features showed a similar diagnostic value to that of visual analysis by radiologists. The information gathered by radiologists was flawed due to human vision's intrinsic limitation. The assistance of machine-learning could not improve the performance either.

Among the radiomic features, the grey-level nonuniformity (GLevNonU) is a parameter deriving from the run-length matrix. It estimates the homogeneity of the pixel grey-level distribution of the tissue. Higher value represents more heterogeneity [23]. It is calculated for 4 directions. "Vertl" represents "vertical", and "45dgr" represents "slanted at 45 degrees". The higher GLevNonU values in HPC group consisted with previous findings that HPCs exhibited more heterogeneous signal intensities than AMs [7].

The major limitation of this study is the small sample size. It was limited by the low incidence of HPC and AM. Also, the retrospective nature led to the loss of some needed information, thus further restricted the sample size and resulted in the lack of a validation data set. Moreover, we attempted to train a classifier on combined features from all sequences, as well as an integrated model including both texture and semantic features. However, these combination brought in a large number of features, while our sample size was relatively too limited, even if *P*-value correction for multiple testing was applied, thus the problem of overfitting was inevitable. Last, no testing of robustness of the radiomics features was performed. It was reported that non-robustness of features did not necessarily denote poor diagnostic performance, since changes in absolute values of features do not evidently alter their relative order, thus it was believed by some researchers that robustness of radiomics features in absolute-scale should not be over-emphasized [24]. In our case, only one MRI scan of each patient was obtained before surgery due to the retrospective nature, so test-retest was unfeasible here. We are looking forward to further carrying out prospective researches with larger scale in the future to fix the flaws above and better illustrate our method in the future.

Conclusion

For discrimination between HPC and AM, TA based on enhanced T1 W images provides the best diagnostic performance among useful sequences, and is better than that of radiologists. It can serve as a practical tool to be used whenever conventional MRI sequences are available.

Authors' statement

Dr. Li: writing.
Dr. Lu: conceptualization.
Dr. Yin: supervision.
Dr. Geng: funding acquisition.
Dr. Xiong: methodology.
Dr. Wang & Dr. Kuai: data curation.
Dr. She: formal analysis.

Disclosure of interest

The authors declare that they have no competing interest.

All authors have reached an agreement that Dr. Li and Dr. Lu are listed as first co-authors. Dr. Yin and Dr. Geng are the corresponding authors of this article.

Acknowledgment

This project was supported by the National Natural Science Foundation of China (Grant No. 81501435), Shanghai Sailing Program (Grant No. 18YF1403000), Shanghai Natural Science Foundation (Grant No. 18ZR1405700) and Science and Technology Commission of Shanghai Municipality (Grant Nos. 16410722800, 17411953700).

Appendix A. Supplementary data

Supplementary data associated with this article can be found, in the online version, at https://doi.org/10.1016/j.neurad.2019.05.013.

References

[1] Stout AP, Murray MR. Hemangiopericytoma – a vascular tumor featuring Zimmermann's pericytes [J]. Ann Surg 1942;116(1):26–33.
[2] Louis DN, Perry A, Reifenberger G, et al. The 2016 World Health Organization Classification of Tumors of the Central Nervous System: a summary [J]. Acta Neuropathol 2016;131(6):803–20.
[3] Sunk KS, Moon JH, Kim EH, et al. Solitary fibrous tumor/hemangiopericytoma: treatment results based on the 2016 WHO classification [J]. J Neurosurg 2018:1–8.
[4] Hasselblatt M, Nolte KW, Paulus W. Angiomatous meningioma – a clinicopathologic study of 38 cases [J]. Am J Surg Pathol 2004;28(3):390–3.
[5] Wu W, Shi JX, Cheng HL, et al. Hemangiopericytomas in the central nervous system [J]. J Clin Neurosci 2009;16(4):519–23.
[6] Liu L, Yin B, Geng DY, et al. Comparison of ADC values of intracranial hemangiopericytomas and angiomatous and anaplastic meningiomas [J]. J Neuroradiol 2014;41(3):188–94.
[7] Meng Y, Chaohu W, Yi L, et al. Preoperative radiologic characters to predict hemangiopericytoma from angiomatous meningioma [J]. Clin Neurol Neurosurg 2015;138:78–82.
[8] Kumar V, Gu Y, Basu S, et al. Radiomics: the process and the challenges [J]. Magn Reson Imaging 2012;30(9):1234–48.
[9] Kassner A, Thornhill RE. Texture analysis: a review of neurologic MR imaging applications [J]. AJNR Am J Neuroradiol 2010;31(5):809–16.
[10] Ernest LH, Richard PK, Samuel JD. A survey of preprocessing and feature extraction techniques for radiographic images [J]. IEEE Trans Comput 1971;20:1032–44.
[11] Shi Z, Zhu C, Degnan AJ, et al. Identification of high-risk plaque features in intracranial atherosclerosis: initial experience using a radiomic approach [J]. Eur Radiol 2018.
[12] Coroller TP, Bi WL, Huynh E, et al. Radiographic prediction of meningioma grade by semantic and radiomic features [J]. PLoS One 2017;12(11):e0187908.
[13] Tustison NJ, Avants BB, Cook PA, et al. N4ITK: improved N3 bias correction [J]. IEEE Trans Med Imaging 2010;29(6):1310–20.
[14] Strzelecki M, Szczypinski P, Materka A, et al. A software tool for automatic classification and segmentation of 2D/3D medical images [J]. Nucl Inst Meth Phys Res Sect A 2013;702:137–40.
[15] Kursa M, Rudnicki W. Feature selection with the Boruta Package [J]. J Stat Software 2010;36(11):1–13.
[16] Kuhn M. Building predictive models in R using the caret package [J]. J Stat Software 2008;28(5):1–26.
[17] Goel A, Kothari M. Hemangiopericytoma of meninges – a "malignant" challenge [J]. World Neurosurg 2015;83(5):767–8.
[18] Chen Q, Chen XZ, Wang JM, et al. Intracranial meningeal hemangiopericytomas in children and adolescents: CT and MR imaging findings [J]. AJNR Am J Neuroradiol 2012;33(1):195–9.
[19] Wang C, Xu Y, Xiao X, et al. Role of intratumoral flow void signs in the differential diagnosis of intracranial solitary fibrous tumors and meningiomas [J]. J Neuroradiol 2016;43(5):325–30.
[20] Uttley D, Clifton AC, Wilkins PR. Haemangiopericytoma: a clinical and radiological comparison with atypical meningiomas [J]. Br J Neurosurg 1995;9(2):127–34.
[21] Liu Z, Wang C, Wang H, et al. Clinical characteristics and treatment of angiomatous meningiomas: a report of 27 cases [J]. Int J Clin Exp Pathol 2013;6(4):695–702.
[22] Chiechi MV, Smirniotopoulos JG, Mena H. Intracranial hemangiopericytomas: MR and CT features [J]. AJNR Am J Neuroradiol 1996;17(7):1365–71.
[23] Baessler B, Mannil M, Maintz D, et al. Texture analysis and machine-learning of non-contrast T1-weighted MR images in patients with hypertrophic cardiomyopathy – Preliminary results [J]. Eur J Radiol 2018;102:61–7.
[24] Lv W, Yuan Q, Wang Q, et al. Robustness versus disease differentiation when varying parameter settings in radiomics features: application to nasopharyngeal PET/CT. Eur Radiol 2018;28:3245.